Climate Dynamics
https://doi.org/10.1007/s00382-023-06834-3

Using an ensemble nonlinear forcing singular vector data assimilation approach to address the ENSO forecast uncertainties caused by the "spring predictability barrier" and El Niño diversity

Yingcong Zheng[1,2] · Wansuo Duan[1,2] · Lingjiang Tao[3] · Junjie Ma[1,2]

Received: 21 December 2022 / Accepted: 17 May 2023

Abstract
An ensemble data assimilation approach for El Niño-Southern Oscillation (ENSO) forecasting is proposed by embedding nonlinear forcing singular vector-data assimilation (NFSV-DA) in the Zebiak–Cane model. This approach generalizes the NFSV-DA performed over a long time series of sea surface temperature anomaly (SSTA) to an ensemble NFSV-DA (EnNFSV-DA) that combines useful precursory signals existed additionally on different decades for ENSO predictions. With the EnNFSV-DA of the Zebiak–Cane model, the SSTA associated with ENSO events during 1961–2020 is predicted. It is shown that the ENSO forecasts made by the EnNFSV-DA outperform the control forecasts generated by a coupled initialization procedure and also the forecasts made by the NFSV-DA, and with the lead times of skillful forecasting being extended from less than 6 months in the control forecast and 10 months in the NFSV-DA to more than 12 months in the EnNFSV-DA. Furthermore, the "spring predictability barrier" (SPB) that severely limits ENSO forecasting becomes very weak in the predictions generated by the EnNFSV-DA of the Zebiak–Cane model. It is also encouraging that the use of the EnNFSV-DA can identify the warm signal in the equatorial central Pacific at a lead time of 8 months, which has a strong capacity to distinguish the types of El Niño events in predictions. Therefore, the EnNFSV-DA could be a useful DA approach to address both initial and model error effects and to significantly reduce the SPB phenomenon, especially in recognizing the types of El Niño in predictions.

Keywords ENSO prediction · Data assimilation · Ensemble nonlinear forcing singular vector-data assimilation · ENSO diversity · Spring predictability barrier

1 Introduction

El Niño-Southern Oscillation (ENSO) has strong influences on global weather and climate (Alexander et al. 2002; Cane 1984; McPhaden et al. 2006). However skillful ENSO predictions are presently only able to achieve 6-month lead time (Chen and Cane 2008; Tang et al. 2018). In particular, a new type of El Niño events have occurred frequently since the 1990s and make the ENSO more diverse with eastern Pacific (EP)- and central Pacific (CP)-El Niño events (Ashok et al. 2007; Kao and Yu 2009; Kug et al. 2009), which further increases the uncertainties in ENSO predictions (Barnston et al. 2012; Duan and Mu 2018; Ham and Kug 2012; Tao and Duan 2019; Tao et al. 2020). To date, most of the existing models remain unable to exhibit the diversity of El Niño types while still producing lower forecasting capabilities for CP El Niño events (Ham and Kug 2012; Hendon et al. 2009; Jeong et al. 2012; Kim et al. 2012; Ren et al. 2019; Zheng and Yu 2017).

Initial errors have a significant effect on the forecasting uncertainties of ENSO [see the reviews of Duan and Mu (2018) and Tang et al. (2018)]. Data assimilation approaches have been applied to reduce the effect of initial errors for ENSO forecasts (Chen et al. 1997; Gao et al. 2016; Keenlyside et al. 2005; Tang et al. 2004); especially, it has been

✉ Wansuo Duan
duanws@lasg.iap.ac.cn

[1] LASG, Institute of Atmospheric Physics, Chinese Academy of Sciences, Beijing 100029, China

[2] University of Chinese Academy of Sciences, Beijing 100049, China

[3] School of Marine Sciences, Nanjing University of Information Science and Technology, Nanjing 210044, China

Published online: 01 June 2023

suggested that assimilating additional targeted observations in sensitive areas can obtain more accurate initial values, then more accurate ENSO predictions (Duan et al. 2018; Kramer and Dijkstra 2013; Langland 2005; Mu et al. 2015; Snyder 1996). However, for El Niño-type diversity, increasing attention has been given to modeling error effects on ENSO forecasting. For example, Duan et al. (2014) demonstrated that the Zebiak–Cane model (Zebiak and Cane 1987) presents an SST cold-tongue cooling bias that provides the condition for the frequent occurrence of CP El Niño events; Tao et al. (2020) improved the ability to distinguish the El Niño types of an ENSO model by correcting relevant atmospheric and ocean processes. In fact, model errors can be from the absence of some physical processes for simplified models, subgrid processes, atmospheric noise, and so on (Kleeman and Moore 1997; Lopez and Kirtman 2014; Moore and Kleeman 1999; Qi et al. 2017; Yu et al. 2003). Furthermore, these wide range sources of model errors interact and make it impossible to separate their effects and analyze each of them individually (Barkmeijer et al. 2003; Nicolis et al. 2009; Vannitsem and Toth 2002). To address this dilemma, Duan and Zhou (2013) developed a nonlinear forcing singular vector (NFSV) approach, which represents the combined model error that leads to the largest deviation from a reference state in a nonlinear model (Duan and Zhao 2015; Duan and Zhou 2013). The NFSV-type tendency perturbation can identify the spatial structure of the model errors that have the largest effect on prediction uncertainties because NFSV considers the effect of nonlinearities (Duan and Zhao 2015; Tao et al. 2022).

Encouraged by the idea of NFSV, the review of Duan et al. (2022) proposed an NFSV-data assimilation (NFSV-DA) approach that can offset the effect of prediction errors caused by both initial and model errors [also see Tao et al. (2020)]. By the idea of NFSV-DA, Duan et al. (2014) corrected the Zebiak–Cane model and reproduced two types of El Niño events. Duan et al. (2018) further used this corrected model and provided the optimal observing array for dealing with the challenge of ENSO predictions due to El Niño diversity. Despite these advances in NFSV-DA applications, they always remain in the scenario of ENSO simulations rather than predictions due to the difficulties that NFSV-DA has to adopt the observations during the prediction period when observations are absent. To realize the application of NFSV-DA in predictions, Tao and Duan (2019) innovatively trained a lead-lag relationship between the initial sea surface temperature anomaly (SSTA) and NFSV-type tendency perturbation generated by NFSV-DA, then promoted the NFSV-DA to real-time predictions of El Niño events and achieved high forecasting skill for ENSO [see the review of Duan et al. (2022)].

The lead-lag relationship between the initial SSTA and NFSV-type tendency perturbation constructed by Tao and Duan (2019) was obtained through a singular value decomposition [SVD; Bretherton et al. (1992)] method. The SVD method aims to extract the information that describes the relationship between two variables during a time period (i.e., the training period hereafter) at a large scale. Then, if the training period for SSTA is long enough that the multi-decade information is included, the SVD only identifies the statistically significant components of the relationships from different years and decades. As a result, the SVD may filter out the relationships that occur among a few decades but not statistically significant during the whole training period. In fact, these relationships may be useful for predicting one leading state from a backward state on these decades (see Sect. 3). In the present study, we attempt to contain these filtered relationships existed in some decades, in addition to the trained lead-lag relationship during the whole period. This encourages to propose an ensemble NFSV-DA (EnNFSV-DA; see Sect. 3) approach for improving the ENSO prediction, especially for the El Niño diversity forecasting skill. In addition, the ENSO forecasting is also limited by the spring predictability barrier (SPB) phenomenon, which remains unresolved. The SPB almost becomes an essential feature of ENSO forecasting, which often results in the ENSO forecasting skill to decline rapidly during the spring season for predictions that occur before spring (Duan and Wei 2013; Webster and Yang 1992). Quite a few studies emphasized the important role of initial errors in yielding the SPB [see the review of Duan and Mu (2018)]; simultaneously, and there exist other studies that argued that model errors can also cause an SPB for ENSO events (Tao et al. 2019; Wu et al. 1993). In any case, the EnNFSV-DA approach that is developed can offset the effect of initial and model errors. However, can this method eliminate the effect of the SPB? In the present study, we attempt to also address this question.

The paper is organized as follows. Section 2 introduces the Zebiak–Cane model and associated observations adopted in the present study. Section 3 proposes the EnNFSV-DA approach to predict ENSO using the Zebiak–Cane model. Section 4 shows the performance of the EnNFSV-DA in forecasting Niño3.4 index especially explores the ability to predict which type of El Niño will occur and eliminate the SPB. Finally, a summary and discussion are provided in Sect. 5.

2 Zebiak–Cane model and associated observations

The intermediate coupled Zebiak–Cane model is adopted in the present study, which is an anomaly model consisting of a Gill-type steady-state linear atmospheric model and a reduced-gravity ocean model, and depicts the thermodynamic anomaly of the tropical Pacific with oceanic and atmospheric anomalies

near the mean climatological state specified from observations (Zebiak and Cane 1987). This is the first coupled ocean-atmosphere model to successfully simulate observed ENSO interannual variability. Since wined the fame for predicting the 1986–1987 El Niño event, the Zebiak–Cane model has been widely adopted to study ENSO dynamics and predictability (Blumenthal 1991; Duan et al. 2014, 2022; Tang et al. 2008; Tao and Duan 2019; Xue et al. 1994). In the present study, we also use this model to explore the use of EnNFSV-DA in improving the capacity of ENSO forecasting. Note that the Zebiak–Cane model used here is the original version because its adjoint for the calculation of the NFSV-DA is ready [see section 3; Xu et al. (2006)], but the bias correction term used in the latest version of Lamont–Doherty Earth Observatory model [LDEO5; Chen et al. (2004)] has been adopt in this study to improve the forecasting skill in the Zebiak–Cane model.

The ERSST.v5 data (Huang et al. 2017) are used to initialize the Zebiak–Cane model for prediction via a coupled nudging scheme, where this initialization scheme can bring air-sea coupling information to model initial field and has been thought of as an effective initialization scheme of the Zebiak–Cane model by Chen et al. (2004). The ERSST.v5 data is a global monthly dataset that spans from 1854 to the present and has spatial coverage over 88.0°N–88.0°S, 0.0°E–358.0°E, with a grid spacing of 2°(longitude)× 2°(latitude).

3 The formulation of the EnNFSV-DA for the Zebiak–Cane model

Duan et al. (2022), as mentioned in the introduction, proposed the NFSV-DA that considers the combined effect of initial error and model errors and calculates the total tendency perturbation that produces model results close to observations at a given lead time [also see Tao and Duan (2019)]. Specifically, for a forecast model, its equations can be expressed as in Eq. (1).

$$\begin{cases} \frac{\partial u}{\partial t} = F(u,t) \\ u|_{t=0} = u_0 \end{cases} \tag{1}$$

where u is a forecast variable contaminated by initial and model errors, u_0 is its initial state including errors, F is a nonlinear operator describing dynamical and physical laws for controlling the motions of u and the combined effects of kinds of model errors are contained in it, and t is the time. Suppose that M is the propagation of Eq. (1), the numerical solution of Eq. (1) at time t can be described as in Eq. (2),

$$u(x,t) = M_t(u_0) \tag{2}$$

With a disturbance f superimposed on the model tendency, Eq. (1) can be rewritten as in Eq. (3)

$$\begin{cases} \frac{\partial u}{\partial t} = F(u,t) + f \\ u|_{t=0} = u_0 \end{cases} \tag{3}$$

Then its solution $u(x,t)$ is as follows.

$$u(x,t) = M_t(f)(u_0) \tag{4}$$

Then, NFSV-DA applies to Eq. (4) and defines a tendency perturbation f^* by Eq. (5).

$$J(f^*) = \min_f \left\| M_t(f)(u_0) - u^{obs}(x,t) \right\| \tag{5}$$

where $u^{obs}(x,t)$ is the observation, $\|\cdot\|$ is a norm for measuring the departure of the results of the perturbed model from the observation, and other mathematical signs are as in Eqs. (1, 2, 3, 4). The Eq. (4) indicates that the tendency perturbation f is superimposed on each time step of model integration to neutralize the errors in the forecast variable u; however, these errors are caused by both initial and model errors. Therefore, the Eq. (5) solves the tendency perturbation f^* that can offset the forecast error caused by both initial and model errors to the highest possible extent and produces the model results that are closest to the observations at time t, although the erroneous initial fields are not optimized for that specific purpose in the Eq. (5).

Regarding ENSO forecasting in the present study, we are concerned with the forecast of the SSTA field and therefore attribute the combined effect of the kinds of model errors to the SSTA tendency (this means that the perturbation is superimposed on the tendency of the SSTA equation). The corresponding NFSV-DA problem is defined as in Eq. (6).

$$J\left(f^*_{t_n}\right) = \min \left\| X\left(f_{t_n}, u_{t_{n-1}}\right) - X^{obs}\left(t_n\right) \right\| \tag{6}$$

where X signifies the SSTA, $[t_{n-1}, t_n]$ with $n = 1, 2, 3 \ldots$ represent assimilation windows, $u_{t_{n-1}}$ describes the variables outputted by the Zebiak–Cane model at time t_{n-1}, and $f^*_{t_n}(n = 1, 2, 3 \ldots)$ is the NFSV-type tendency perturbation we seek to make the model SSTA closest to the observation during the assimilation window $[t_{n-1}, t_n]$.

We generate initial fields of the Zebiak–Cane model for a total of 589 months from 1960.12 to 2009.12 using the coupled initialization procedure mentioned in Sect. 2. Using these initial fields, we referred to Tao and Duan (2019) and calculated the NFSV-type tendency perturbations according to Eq. (6) using the spectral projected gradient algorithm [SPG2; Birgin et al. (2000)], where the adjoint of the Zebiak–Cane model is used to calculate the gradient of the cost function Eq. (6) with the tendency perturbation f. When the forecast period is 1 year, 12 NFSV-type tendency perturbations $f = (f_{t_1} \ldots f_{t_{12}})$ are obtained with the assimilation window $[t_{n-1}, t_n]$ be one month in length, for a given initial time of the forecast. From each of the initial fields during the

period from December 1960 to December 2009, we integrate forward for 1 month and solve Eq. (6) with $n=1$ such that the model SSTA is closest to the observation at time t_1, and f_{t_1} is obtained; with the model initial field being corrected by f_{t_1} at time t_1, we continue to integrate forward for 1 month and solve Eq. (6) with $n=2$, obtain f_{t_2}, and so on, where we finally obtain $f=(f_{t_1},f_{t_2},\ldots f_{t_{12}})$. This outcome indicates that each monthly NFSV-type tendency perturbation is generated from the respective state field at the beginning of the month, which has been corrected by the tendency perturbations f_{t_n} before this month. For convenience, we plot in Fig. 1 a sketch diagram of the NFSV-type tendency perturbations $f=(f_{t_1},f_{t_2},\ldots f_{t_{12}})$ generated by NFSV-DA for different initial months. A composite analysis was performed on the components of $f=(f_{t_1},f_{t_2},\ldots f_{t_{12}})$ whose months overlap for different initial months; then, a total of 600 composite NFSV-type tendency perturbations were obtained from 1961.1 to 2010.12, which are also plotted in Fig. 1.

We adopt the method of Ashok et al. (2007) to classify types of El Niño events; then nine EP El Niño and eleven CP El Niño events are predetermined (see Table 1). The components of the NFSV-type tendency perturbations during EP and CP El Niño mature phase (i.e., the period from November to December and then to next January; NDJ) are displayed in Fig. 2. It is seen that either for EP or CP El Nino events, the NFSV-type tendency perturbations often exhibit large anomalies over the central tropical Pacific, sometimes prolonging to the east along the equator, although those of CP El Nino events are more scattered in distribution. This is probably because the amplitudes of SSTA over the areas of large NFSV-type tendency perturbations simulated by the Zebiak–Cane model have large errors, and a much large tendency perturbation should be superimposed to offset them. The relationship between the monthly analysis SSTA made by the Zebiak–Cane model with the coupled nudging scheme in Chen et al. (2004) and the corresponding NFSV-type tendency perturbations $f=(f_{t_1},f_{t_2},\ldots f_{t_{12}})$ along the equator (see Fig. 3) is further examined. It is found that the NFSV-type tendency perturbations also present an ENSO-oscillation over the east tropical Pacific, like that shown in the analysis SSTA. Furthermore, it can also be seen that the monthly dependent NFSV-type tendency perturbations tend to exhibit a "seesaw-effect" with cooling and warming cycle at eastern and western Pacific during most of the years from 1961 to 2010 and a basin warming along the equator during other years. From the definition of the NFSV-type tendency perturbations in Eq. (6), it is inferred that the predictions made by the Zebiak–Cane model with the coupled nudging scheme underestimate the SSTA over central tropical Pacific but overestimate them over the east tropical Pacific during the years when there are a seesaw-effect as above, while they tend to underestimate the SSTA along the whole equator during the years of a basin warming effect. Obviously, this is due to effect of both initial and model errors, and the NFSV-type tendency perturbations could offset these errors effects. Furthermore, from this it is known that the relationship between the NFSV-type tendency perturbations and the analysis SSTA made by the Zebiak–Cane model with the coupling nudging scheme is flow dependent, which encourages us to construct an equation similar to Tao and Duan (2019) that addresses this relationship. Then, we can use this equation to forecast future NFSV-type tendency perturbations according to the analysis SSTA made by the Zebiak–Cane model with the coupling nudging scheme.

Now we construct the equation to forecast the future NFSV-type tendency perturbations of the Zebiak–Cane model when it is integrated for predictions with relevant analysis field as initial value.

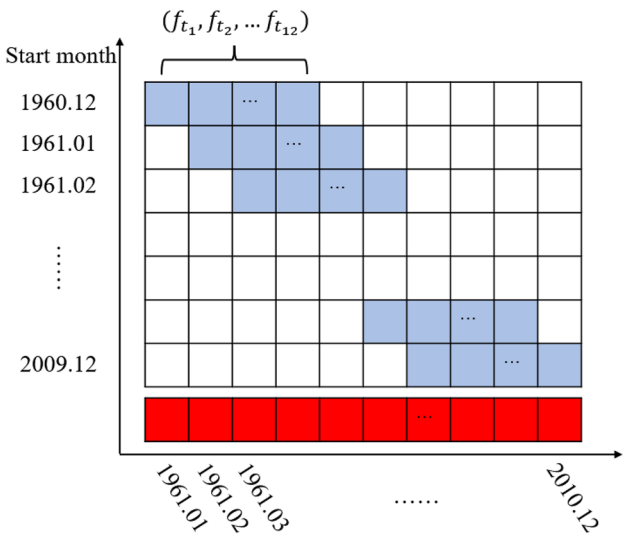

Fig. 1 Schematic diagram illustrating the prediction period, together with its NFSV-DA windows, and the strategy of the composite NFSV-tendency perturbations. The 12 blue shaded boxes in each row cover one prediction period of 12 months, and each month is an NFSV-DA window, corresponding to 12 members of the NFSV-tendency perturbations of one year lead time. The vertical axis marks the start months of the predictions at a one-year lead time. The red shaded boxes on the last row represent the 600 NFSV-tendency perturbations during 1961.1–2010.12, which were obtained by taking the mean of the NFSV members whose assimilation windows overlap for different initial months

Table 1 Two types of El Niño years

Events	The year when the event peaks
EP El Niño	1969, 1972, 1976, 1982, 1986, 1993, 1997, 2006, 2015
CP El Niño	1963, 1965, 1968, 1977, 1987, 1991, 1994, 2002, 2004, 2009, 2018

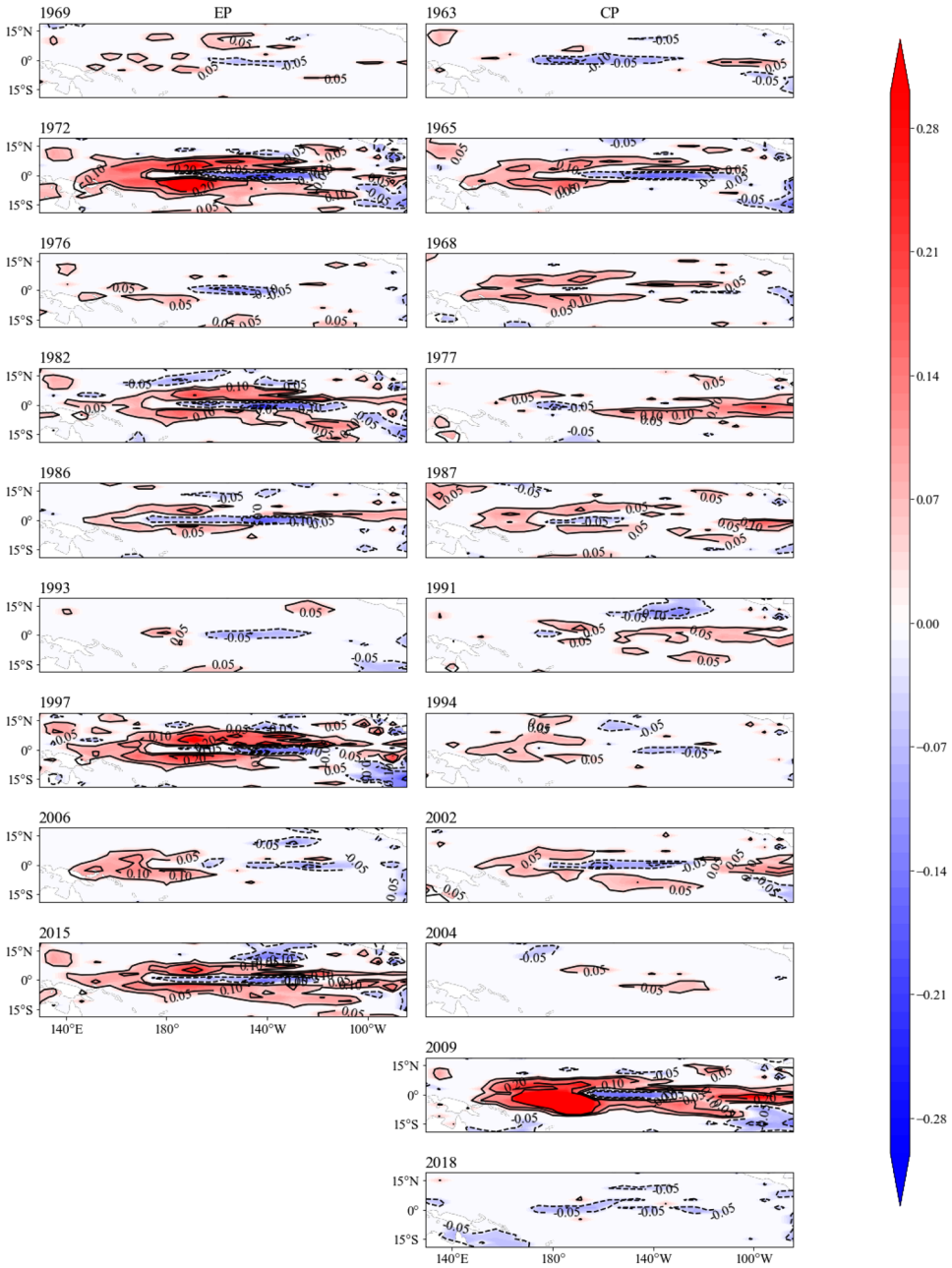

Fig. 2 Horizontal distribution of the NFSV-type tendency perturbations of each of EP and CP El Nino events during their mature phase

These 600 NFSV-type tendency perturbations calculated for the period from 1961.1 to 2010.12 (see Fig. 1) are trained with the analysis SSTA to generate a lead-lag relationship between the SSTA and the NFSV-type tendency perturbation through the SVD method. Specifically, a covariance matrix of analysis SSTA and NFSV-type tendency perturbations is constructed as in Eq. (7).

$$C_l(i,j) = \frac{1}{N-1}\sum_{t=t_1}^{t_N} \mathrm{SSTA}(t,i,j)\cdot \mathrm{NFSV}(t+l,i,j), \tag{7}$$

where (i,j) represent the spatial grids, l represents the lagged months of the NFSV-type tendency perturbation relative to the SSTA, and N is the length of the training period. Using the constructed covariance matrix C, according to the SVD technique, the relationship between the NFSV-type tendency perturbation and the SSTA can be easily derived as having the form of Eq. (8).

$$\mathrm{NFSV}_{pre\_l} = F_l(\mathrm{SSTA}), \tag{8}$$

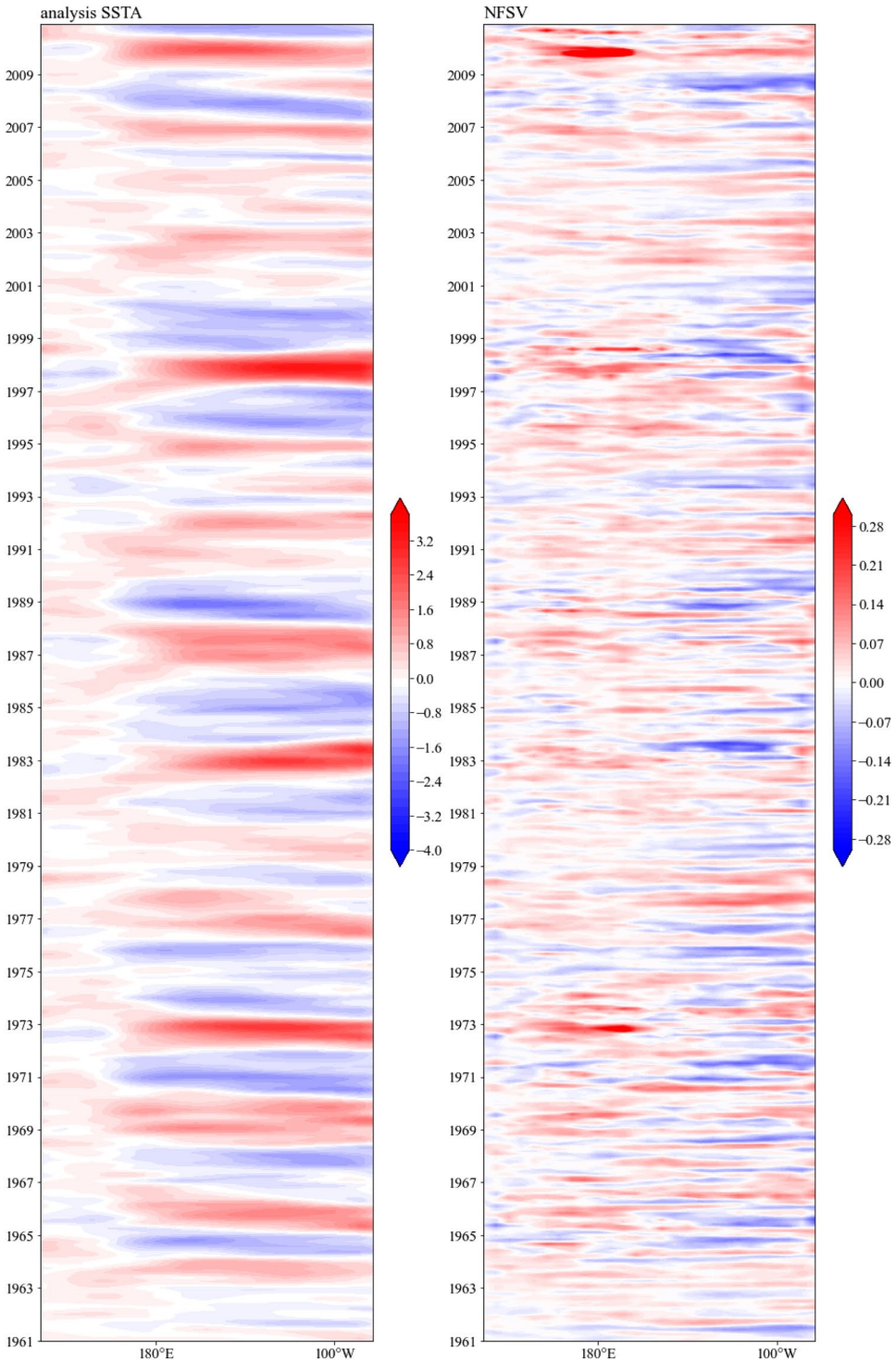

Fig. 3 Time-dependent section along the equator of the analysis SSTA (unit: °C) predicted by the Zebiak–Cane model with the coupling nudging scheme and the NFSV-type tendency perturbations (unit: °C day^{-1})

where F describes the relationship between the SSTA and the NFSV-type tendency perturbation, and NFSV_{pre_l} is the estimated NFSV-type tendency perturbation of the l lagged month.

By experiments, we assign the lagged month $l = 1$ in Eq. (8) for a much higher prediction skill of ENSO. Then, the estimate of the NFSV-type perturbation used to offset the prediction error can be monthly updated according to the analysis SSTA generated by the corrected model at the beginning of the month.

As argued in the introduction, if the training period for determining the relationship between the SSTA and the NFSV-type tendency perturbation is long enough that multi-decade information is included, the SVD only extracts the

statistically significant components of the relationships for different years and decades, while other relationships that exist in a few decades and may be useful for predicting one lead state from a backward state on these decades could be filtered out. To illustrate this point, we plot in Fig. 4 the correlation coefficient (CC) between the analysis SSTA and the NFSV-type tendency perturbations in January for different decades. This shows that the distribution of the CC changed between decades. For example, over the area of 180° northern equator, the CCs are positive during 1961–1971 and 2001–2010 but negative during the other three decades. Then, the relationship between the SSTA and the NFSV-type

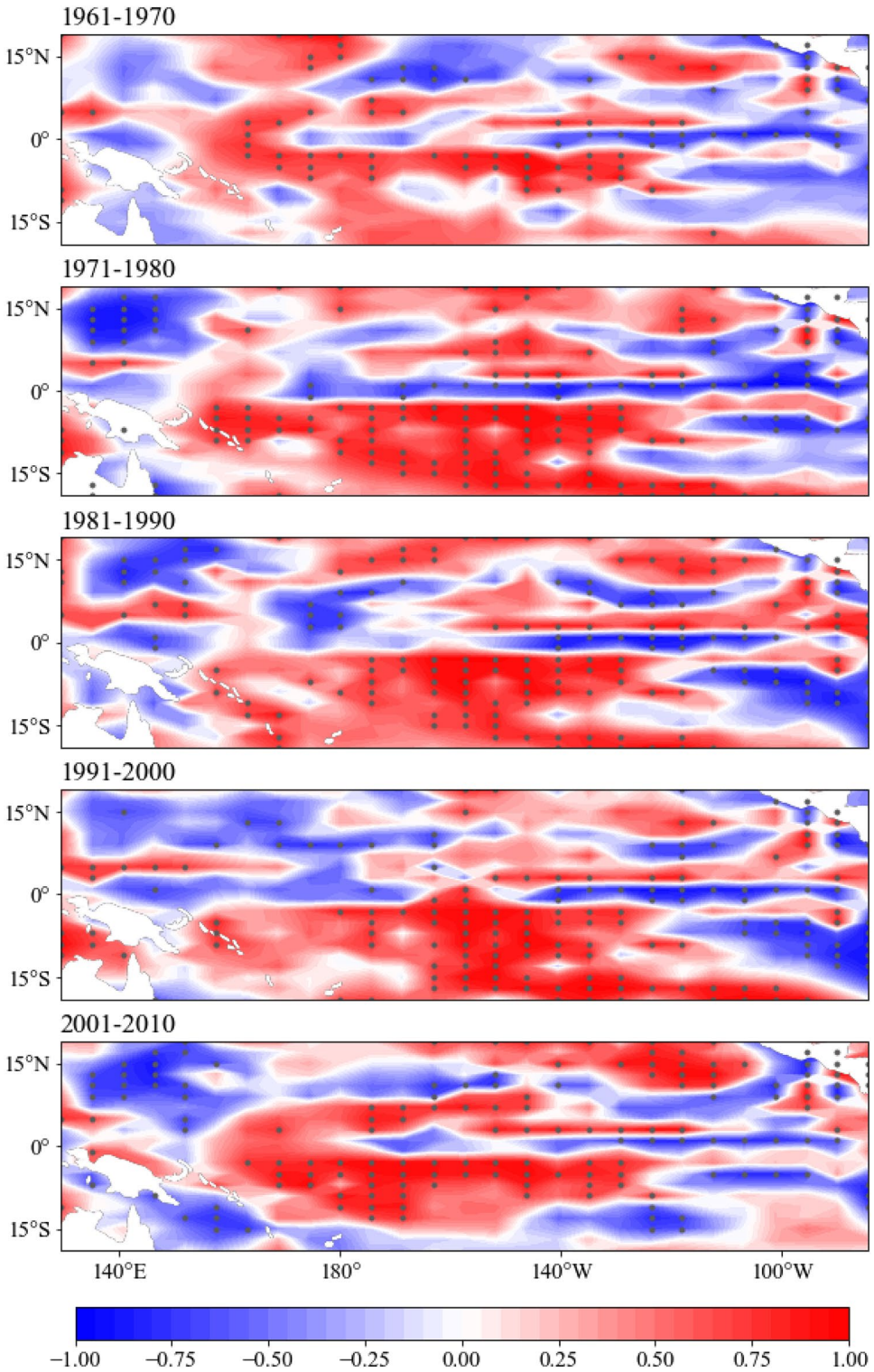

Fig. 4 The correlation coefficient between the SSTA and the NFSV-type tendency perturbations for the month of January during the periods 1961–1970, 1971–1980, 1981–1990, 1991–2000, and 2001–2010. The dotted area is the region that passes the significance test with a 95% confidence level

tendency perturbations during 1961–1970 may help to infer the NFSV-type tendency perturbation during 2001–2010; however, it could be filtered when the SVD was performed for the entire training period since it is not statistically significant for different decades. It is therefore implied that to further improve the ENSO forecasting skill, one should consider this filtered information when using Eq. (8) to deduce the future NFSV-type tendency perturbation. Since such a relationship does not hold for all prediction periods, there may exist uncertainties in ENSO forecasting when using this relationship to generate the NFSV-type tendency perturbation for a given prediction period. To estimate and even reduce the effect of such uncertainties, we propose the ENSO forecasting strategy of EnNFSV-DA. The EnNFSV-DA strategy would first provide the lead-lag relationships between the SSTA and NFSV-type tendency perturbations indicated by Eq. (8) on different decades and then perform an ensemble to the ENSO forecasting results corrected by the estimates of the NFSV-type tendency perturbations derived from these relationships, eventually output a prediction result for ENSO provided by the ensemble mean. As for the specific EnNFSV-DA system for the Zebiak–Cane, it refers to as in Sect. 4.

4 The performance of EnNFSV-DA for ENSO forecasting

We regard 1961–2010 as the whole training period and 2011–2020 as a testing period to examine the ENSO forecasting skills of the EnNFSV-DA. The lead-lag relationships of the NFSV-type tendency perturbations to the model SSTA are constructed through 14 sub-training periods from the whole training period. These periods include five periods of 1961–1970, 1971–1980, 1981–1990, 1991–2000 and 2001–2010, each with a duration of 10 years; four periods of 1961–1980, 1971–1990, 1981–2000 and 1991–2010, each with a duration of 20 years; three periods of 1961–1990, 1971–2000 and 1981–2010, each with a duration of 30 years; and two periods of 1961–2000 and 1971–2010, each with a duration of 40 years. All these 14 periods ensure effective statistics for the SVD approach. The 14 lead-lag relationships yield 14 estimates for the NFSV-type tendency perturbations for a given prediction, which, together with that deduced by the whole training period, compose 15 estimates to the NFSV-type tendency perturbation for a given prediction period for ENSO. With these estimated NFSV-type tendency perturbations, we integrate the Zebiak–Cane model initialized by the coupled initialization scheme to forecast the ENSO and then 15 perturbed forecasting members are obtained. Finally, an ensemble mean is made to these forecasting members to provide a deterministic forecasting result for ENSO. Thus far, the EnNFSV-DA for ENSO forecasting has been finalized in the Zebiak–Cane model. Note that the perturbed forecasting member using the led-lag relationship derived from the whole training period is as that of Tao and Duan (2019), and referred to as TD hereafter for convenience; and the forecast made by the Zebiak–Cane model initialized by the coupled initialization scheme [see section 2 and Chen et al. (2004)] is referred as control forecast. Then the role of the EnNFSV-DA in improving ENSO forecasting skill is evaluated by comparing with the forecasts made by the NFSV-DA (i.e., TD) and the control forecasts. The forecasting skill for ENSO is evaluated in terms of the temporal variability of the Niño3.4 index (i.e., the SSTA averaged for the Nino3.4 region), the spatial variability of tropical SSTA and its associated ENSO diversity. The influence on the SPB that occurred in ENSO forecasting of the EnNFSV-DA is also examined.

4.1 The forecasting skill of SSTA

The forecasting skill of the Niño3.4 index associated with ENSO events is evaluated using the root mean square error (RMSE; see Appendix) and the anomaly correlation coefficient (ACC; see Appendix).

Figure 5 plots the ACC and RMSE of the predicted Niño3.4 index during the training and testing periods. Note that a prediction is thought of as a skillful one if the ACC between the predicted Niño3.4 index and the observations are larger than 0.6 (Barnston et al. 2012; Kirtman and Zebiak 1997; Murphy and Epstein 1989). Figure 5 indicates that the TD prolongs the skillful lead time of the control forecast from 5 to 9 months, while the EnNFSV-DA consistently lasts up to 11 months in the training period. Such improvement appears to be much better during the testing period. Specifically, TD increases the skillful lead time from 4 to 11 months; moreover, the EnNFSV-DA promotes the lead time further to more than 12 months. In terms of the RMSE, regardless of the training or testing period, both TD and EnNFSV-DA achieve an RMSE less than 1.0 at a lead time of 12 months, with the latter having a much smaller RMSE, while the control forecast at a lead time of 6 or 7 months increases to an RMSE near 1.2. It is clear that TD improves the forecasting skill of the control forecast, and EnNFSV-DA further increases it to a much higher level in terms of the predictions of Niño3.4 index, which may illustrate that the EnNFSV-DA extracts useful signals from different decades associated with the SSTA predictions and further reduces their uncertainties in the estimate of future SSTA through an ensemble.

The improvements of the EnNFSV-DA can also be reflected from the predictions of the spatial variability of the tropical SSTA during the training and testing periods. Figure 6 gives the spatial distribution of the ACC between the predicted SSTA and the observed SSTA at lead times of

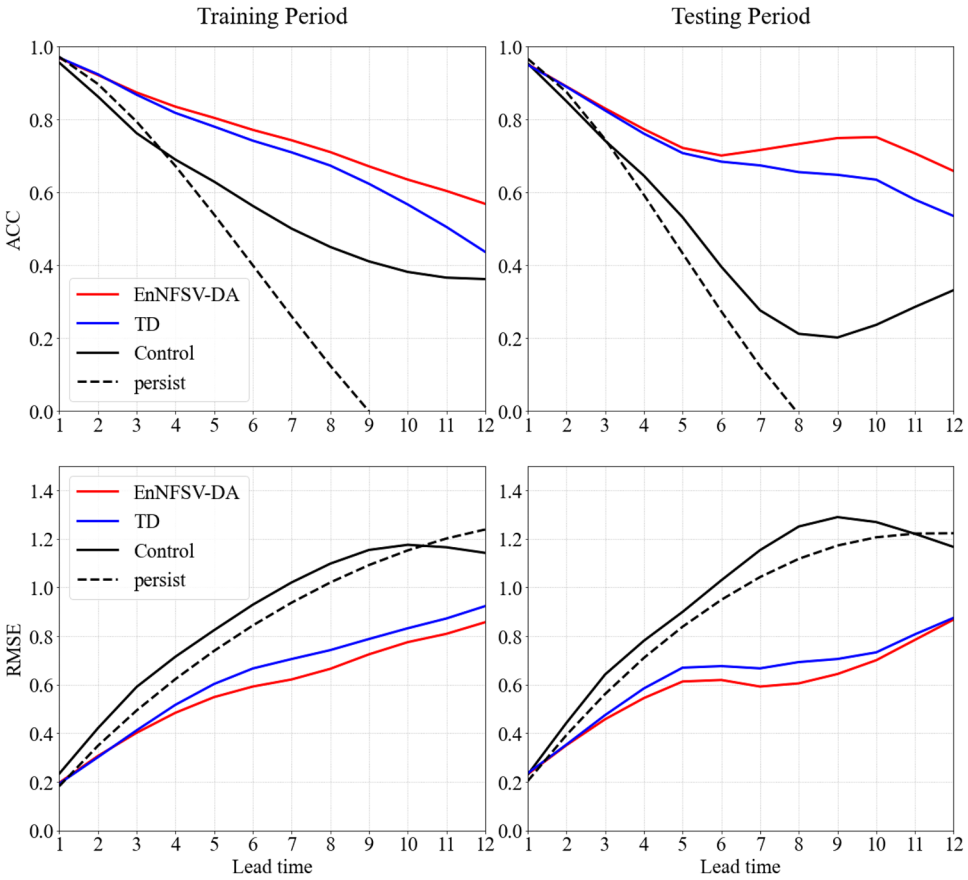

Fig. 5 The ACC and RMSE of predicted Niño3.4 index for the training period (1961–2010) on the left column and the testing period (2011–2020) on the right column. The red line represents the forecast generated by the EnNFSV-DA, the blue line represents the TD, the black solid line represents the control forecast, and the dotted line represents the persistence (color figure online)

3, 6, 9, and 12 months for the training and testing periods. It is shown that both periods present predictions generated by the TD with a higher ACC than the control forecasts for any lead time; even the EnNFSV-DA overtakes these two kinds of predictions, far exceeding the control forecast and achieving a much high forecasting skill. For simplicity, only the details from the testing period will be described. Markedly, when the lead time reaches 6 months, the ACC in the control forecast rapidly decreases to a value slightly larger than 0.6 only in a very small region located in the southeastern tropical Pacific Ocean. However, the TD, when the lead time is larger than 9 months, even reaches to 12 months, still presents an ACC larger than 0.6 in many more regions; further, the EnNFSV-DA provides the regions of the ACC larger than 0.6 that are far more than those of the TD at any lead time; even if the lead time is 12 months, the ACC values are still larger than 0.7 in the northeastern tropical Pacific Ocean.

For the RMSE, we plot in Fig. 7 the noise-to signal—(NS) ratio of the SSTA predictions, which is calculated by taking the ratio of the RMSE of the predicted SSTA to the observed SSTA (see Appendix). A value less than 1.0 of the NS indicates a skillful prediction of the SSTA. By comparing the EnNFSV-DA with the TD and control forecasts, it is found that the EnNFSV-DA presents more regions of NS values less than 1.0 than the TD and control forecasts. Specifically, the NS values in the control forecast are less than 1.0 only in a small region in the southeastern tropical Pacific Ocean at a lead time of 6 months. Although a region with a NS of less than 1.0 for the TD can reach a lead time of 9 months, it is still in a very small area. However, the EnNFSV-DA presents such regions that not only reach the lead time of 9 months but also cover a much broader area (see Fig. 7). Therefore, we show that the EnNFSV-DA also performs much better than the TD and control forecasts for the predictions of the spatial variability of the SSTA associated with ENSO.

It is obvious that for the predictions of temporal-spatial variabilities of the SSTA associated with ENSO events, a unified conclusion was obtained, as both EnNFSV-DA and NFSV-DA significantly improved the forecasting skill of the control forecast; in particular, EnNFSV-DA provides the best performance in promoting the forecasts of the SSTA associated with ENSO events to a higher level.

4.2 The skill of El Niño diversity forecast

Section 4.1 has demonstrated that the EnNFSV-DA has the best performance in the forecasts of the spatial variability of the tropical SSTA compared with the TD and the control

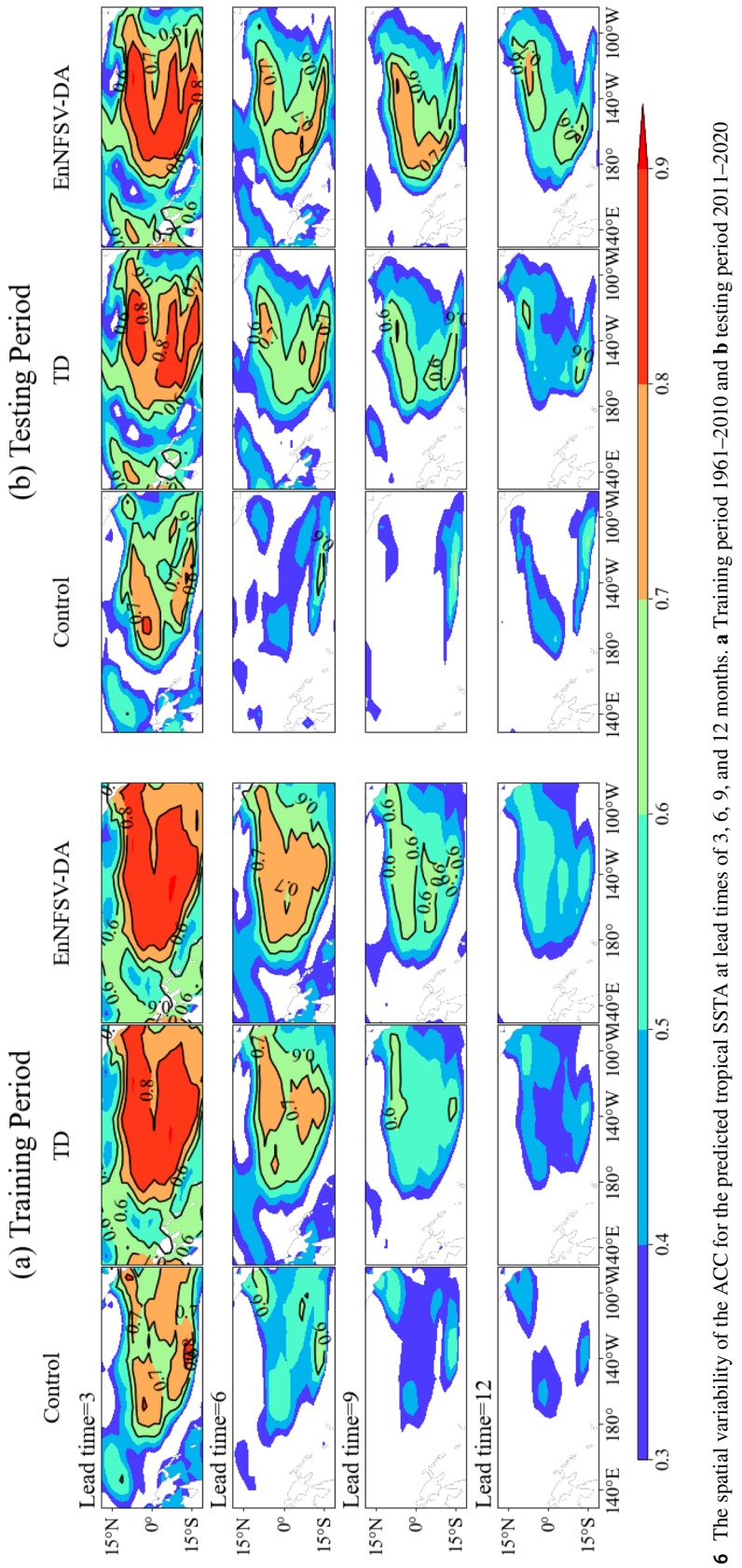

Fig. 6 The spatial variability of the ACC for the predicted tropical SSTA at lead times of 3, 6, 9, and 12 months. **a** Training period 1961–2010 and **b** testing period 2011–2020

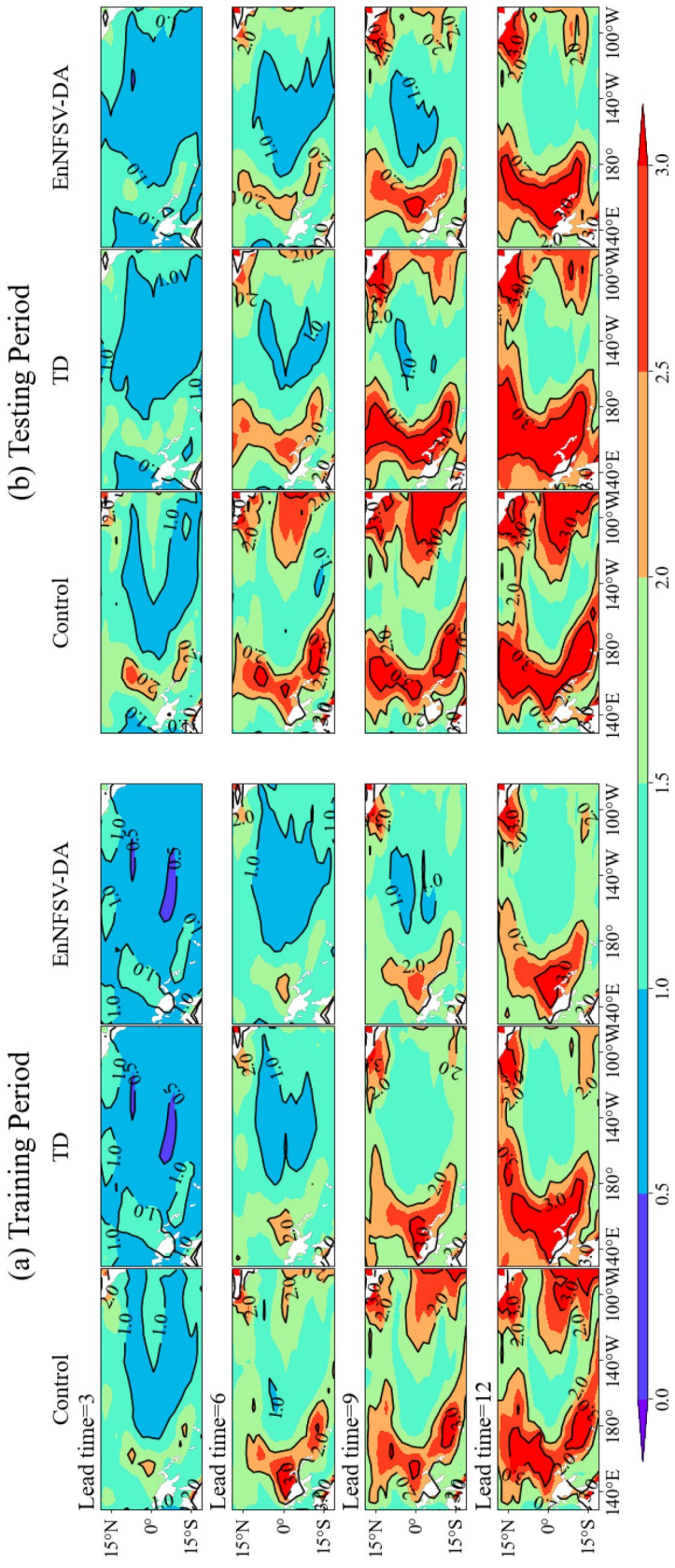

Fig. 7 Similar to Fig. 6 but for the NS

forecast; thus, the question arises of whether the EnNFSV-DA has the ability to identify the types of El Niño events. In this section, we investigate the capacity of the EnNFSV-DA in distinguishing the El Niño types.

A composite is made to the tropical SSTA pattern during the mature phases of EP and CP El Niño events. The capacities of the EnNFSV-DA that identifies the two types of events in predictions are investigated.

It is known that the Zebiak–Cane model only has the ability to simulate typical EP El Niño events even if the advanced four-dimension variational data assimilation (4DVar) was adopted to initialize it (Duan et al. 2014), and therefore, the control forecasts cannot reproduce CP El Niño events [Fig. 8; see also Duan et al. (2014)]. However, from Fig. 8, we can see that the TD recognizes the dominant warm signal in the tropical central Pacific at a lead time 4 of months, while the EnNFSV-DA tends to present a warm center departing from the east but approaching the tropical central Pacific until a lead time of 8 months. Moreover, the spatial CC of the mature phase SSTA between predictions and observations is much higher in the EnNFSV-DA than in the TD, with the former 0.8394 but the latter 0.9 at a lead time of 8 months.

For the EP El Niño events, the control forecasts can identify them up to a lead time of 12 months; however, it is the TD, especially the EnNFSV-DA that are much better at reproducing the EP El Niño events with much higher ACC (see Fig. 9).

From the above, it is shown that the EnNFSV-DA can identify a warm center approaching the tropical central Pacific up to 8 months in advance and be much better at reproducing the EP El Niño events at a lead time of 12 months. This indicates that the types of El Niño events can be distinguished at least 8 months in advance by the EnNFSV-DA, which is far beyond the lead times of 1–4 months demonstrated by Jeong et al. (2012). It is implied that the EnNFSV-DA grasps more signals on distinguishing types of El Niño by considering an ensemble of the linkages between SSTA and the NFSV-type tendency perturbations in different decades. This shows that the

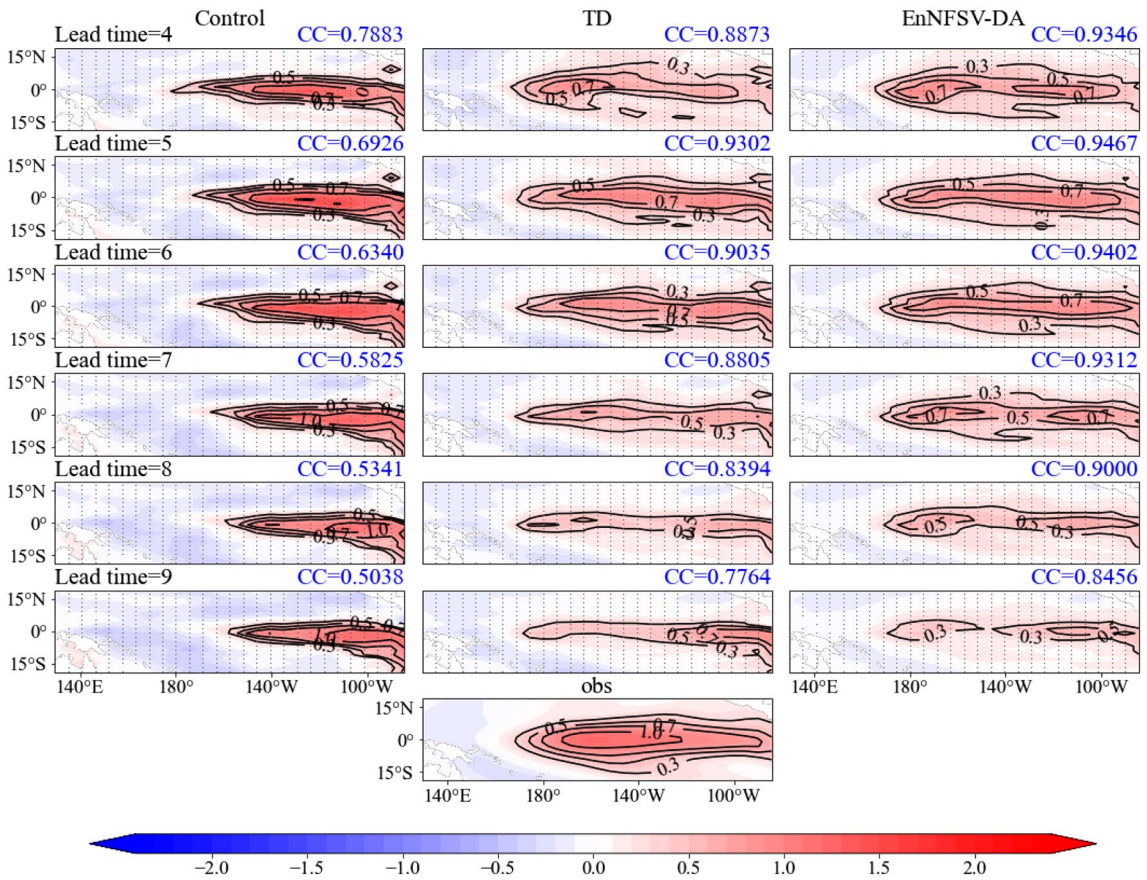

Fig. 8 The composition of mature phases (i.e., the NDJ) SSTA of all typical CP El Niño events during 1961–2020 for the control forecast (left), the TD (middle) and the ensemble mean (here is the median) of the EnNFSV-DA (right) forecasts at lead times of 4, 5, 6, 7, 8, and 9 months. The bottom is the composition of the observed SSTA for the mature phase of the typical CP El Niño events. The gray points in the figure are the areas that passed the significance test with a 95% confidence level. The CC values for each picture are the correlation coefficient of the mature phase SSTA pattern between the prediction and the observation

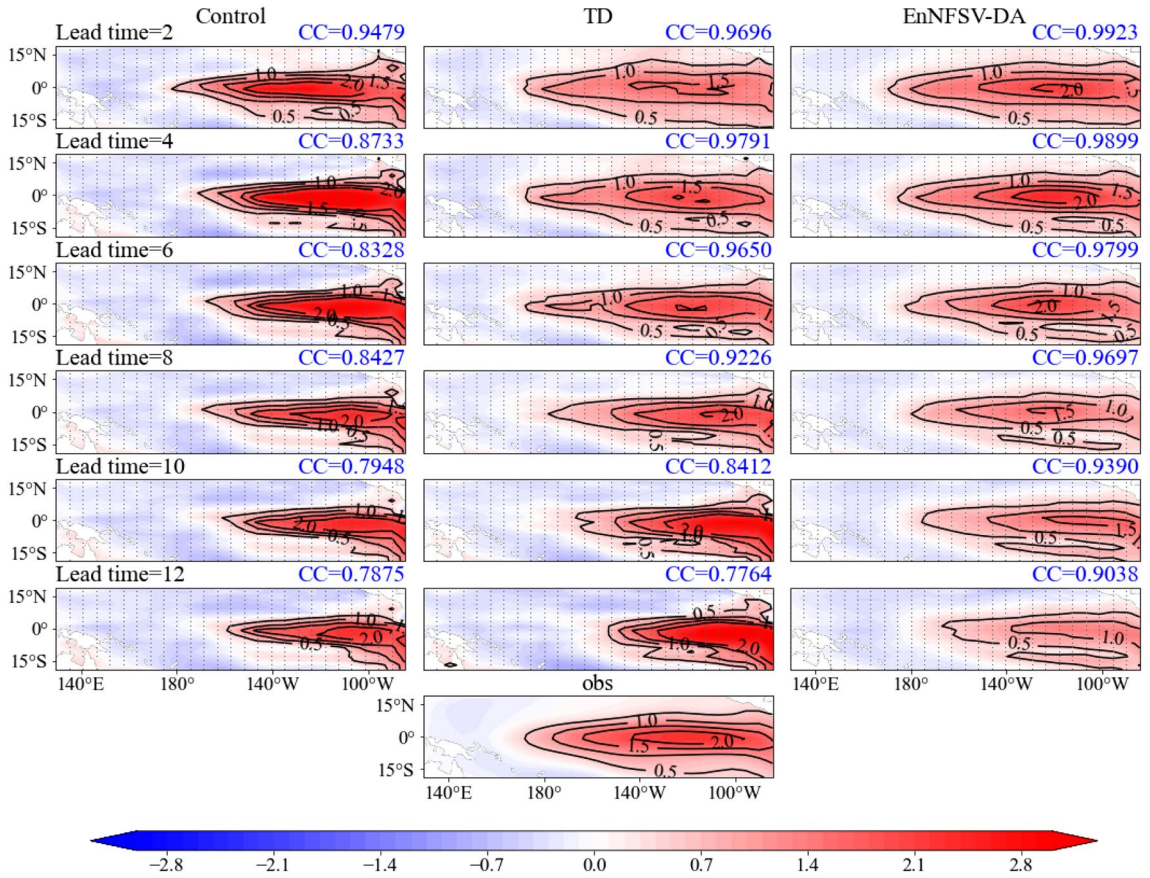

Fig. 9 Similar to Fig. 8 but for EP events at 2-, 4-, 6-, 8-, 10-, and 12-month lead times

EnNFSV-DA has more potential than the TD for predicting which type of El Niño will occur.

The key of the EnNFSV-DA being able to identify El Nino types in predictions lies in that it helps the Zebiak–Cane model predict the CP-El Nino events 8 months in advance. Then how is the Zebiak–Cane model physically corrected by the EnNFSV-DA to output the CP-El Nino events? Figure 10 plots the evolution of the NFSV-type tendency perturbations, SSTA, wind stress anomaly, thermocline depth in both the control forecast and the EnNFSV-DA and their differences, respectively. From Fig. 10, we can see that the SSTA in the control forecast has a significantly cold bias with respect to the observation in the equatorial central Pacific during the mature phase; correspondingly, the composite of the 15 NFSV-type tendency perturbations provided by the EnNFSV-DA tend to have a large scale zonal see-saw structure with positive SSTA tendency in the equatorial western and central Pacific and negative SSTA tendency in the equatorial eastern Pacific during the whole lead time 8 months. Physically, when these perturbations are superimposed to SSTA tendency of the Zebiak–Cane model, they would force the SSTA tendency to warm/cool the SST in the equatorial western and central Pacific/the equatorial eastern Pacific. As a result, the central Pacific SSTA predicted by the EnNFSV-DA would increase against the control forecast while the eastern Pacific SSTA would decrease (see Fig. 10b3), resulting in a stronger warm signal occurring in the central Pacific. The NFSV-type tendency perturbations of the see-saw structure, when they are superimposed to the SSTA tendency, also tend to force an anomalous wind convergence in the central Pacific and an anomalous wind divergence in the eastern Pacific. These anomalous winds would not only help persist the central Pacific warmer SST center but also lead to the deepening of thermocline depth in the central Pacific, which, in turn, is helpful for the SST warming there. Therefore, the relevant tropical sea-air coupling processes during CP El Nino events are corrected by using the EnNFSV-DA, ultimately improving the prediction skills of CP El Nino events.

4.3 The EnNFSV-DA promotes ENSO forecasting bestriding the SPB phenomenon

The SPB phenomenon, as mentioned in the introduction, is an essential feature of ENSO forecasting and often results from the combined effect of initial and model errors. The

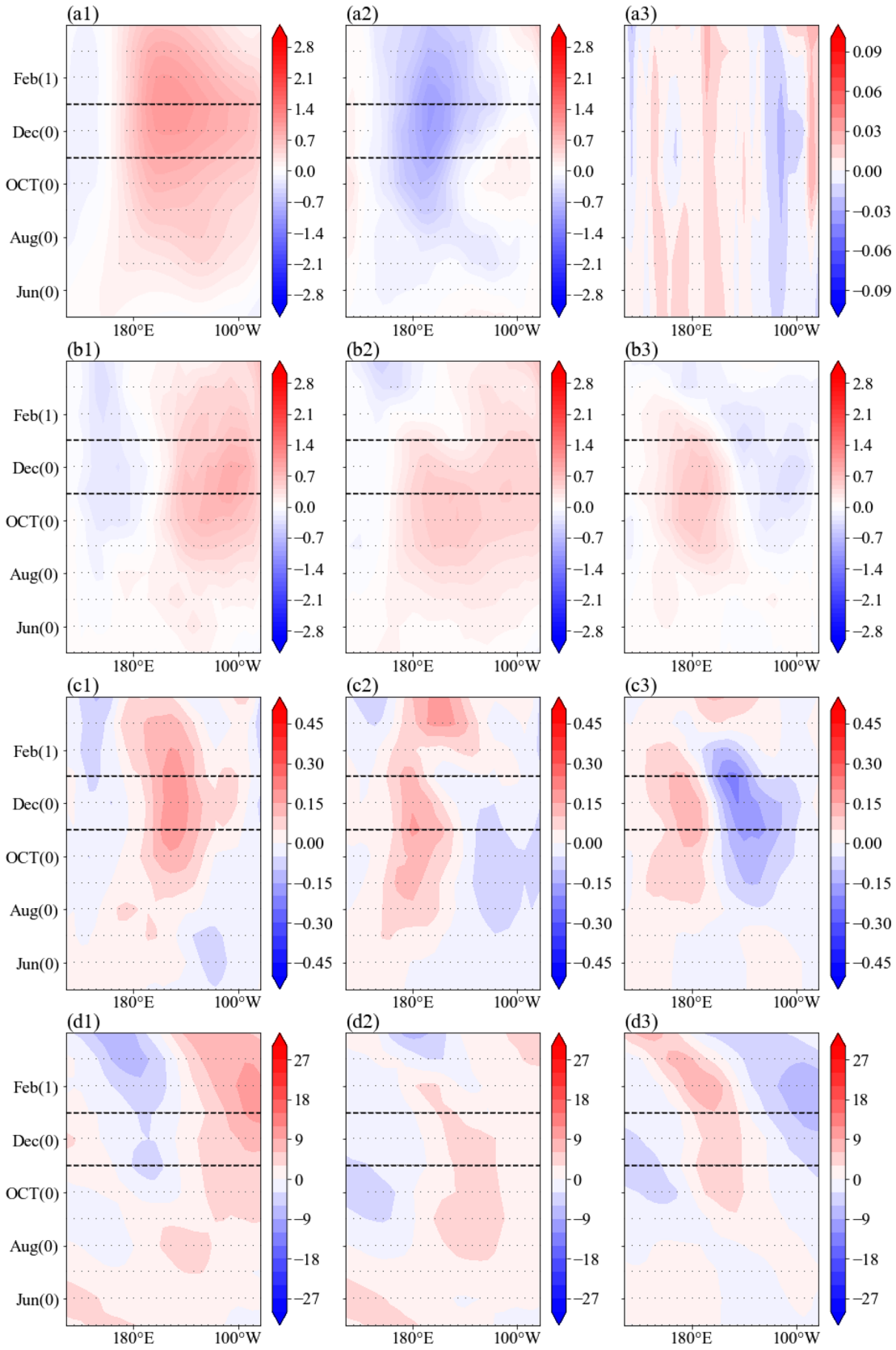
(a1)
(a2)
(a3)
(b1)
(b2)
(b3)
(c1)
(c2)
(c3)
(d1)
(d2)
(d3)
Feb(1)
Dec(0)
OCT(0)
Aug(0)
Jun(0)
180°E
100°W
2.8
2.1
1.4
0.7
0.0
−0.7
−1.4
−2.1
−2.8
0.09
0.06
0.03
0.00
−0.03
−0.06
−0.09
0.45
0.30
0.15
0.00
−0.15
−0.30
−0.45
27
18
9
0
−9
−18
−27

◂**Fig. 10** The composite for the CP El Nino in the present study. **a1** The observed SSTA, **a2** the differences of SSTA between control forecast and observation, **a3** the NFSV-type tendency perturbations provided by EnNFSV-DA; and the evolution of the **b** SSTA and **c** wind stress anomaly and **d** thermocline depth anomaly in control forecast (**1**), EnNFSV-DA (**2**) and the differences (**3**) between EnNFSV-DA and control forecast. The forecasts are initialized at April (0) and have a 8-month lead time. The dashed lines mark the mature phase period of the El Nino. The gray points indicate the region that passed the significance test with a 95% confidence level

EnNFSV-DA, also introduced, plays a role in offsetting the prediction errors caused by both initial and model errors. That is, whatever errors are contained in ENSO forecasting, the EnNFSV-DA would neutralize their effects on prediction uncertainties. To confirm this argument, we plot the forecasting skill of the Niño3.4 index in Fig. 11, which was measured by the ACC as a function of the start and lead times of the predictions. It is shown that the ACC between the control forecasts and the observations drops rapidly, when the predictions span the boreal spring and the beginning of summer (i.e., April–May–June; AMJ), especially during the testing period 2010–2020, which is illustrated by the dense contours of the ACC during the AMJ season. However, the ACC achieved by the TD and the EnNFSV-DA present much higher values; in particular, their contours distribute much more sparsely across the AMJ and indicate a much weak SPB occurring in the predictions made by both TD and EnNFSV-DA. Particularly, it can be easily seen that the EnNFSV-DA, compared with the TD and especially the control forecast, further extends the skillful ACC to a much longer lead time. It is therefore clear that NFSV-DA (i.e., the TD) reduces the impact of SPB by offsetting prediction errors caused by initial and model errors; then the EnNFSV-DA further estimates the uncertainties of the NFSV-DA and successfully significantly reduces the effect of the SPB, finally promoting the forecasting skill for ENSO events measured by the ACC to a much higher level.

The ACC measures the likelihood of two states while the prediction error often investigates how far apart the two states are from each other. From the above, it is known that the EnNFSV-DA enhances the likelihood between the prediction of the SSTA influenced by the SPB and the observations. Then, whether it also corrects the bias of prediction from the observation needs to be determined. To address this issue, we plot in Fig. 12 the seasonal growth rate (see Appendix) of the prediction errors for the lead time of 12 months with the start months January, April, July, and October, respectively.

It is demonstrated that the largest growth rates of the prediction errors occur during AMJ and/or JAS (i.e., July–August–September) in the control forecasts, while the TD often reduces these growth rates. More importantly, the EnNFSV-DA does not present a large growth rate of prediction errors during AMJ and JAS and eases the seasonal fluctuation of the seasonal growth rates especially with much smaller growth rates of prediction errors than the TD at almost all seasons, which obviously weak the SPB phenomenon. Therefore, the EnNFSV-DA significantly reduces the effect of the SPB on ENSO event forecasting.

5 Conclusion and discussion

The NFSV-DA approach proposed by Duan et al. (2022) solves a tendency perturbation that can offset the prediction errors caused by both initial and model errors In ENSO predictions, this kind of tendency perturbations are originally derived by a lead-lag relationship between the initial analysis SSTA and the NFSV-type tendency perturbation that results in model forecasts closest to the observations during the training period. In the present study, the NFSV-DA is further extended to the EnNFSV-DA by considering the contributions of the SSTA signals of different decades (located in the training period). With the application of the EnNFSV-DA to the Zebiak–Cane model, a group of perturbed forecasts for the SSTA associated with ENSO events are obtained; then an ensemble mean of these forecasts is performed to reduce the uncertainties of the contributions of decadal SSTA signals to future SSTA predictions.

It is shown that the ensemble mean, as expected, has a much higher forecasting skill than the forecast provided by the NFSV-DA. Specifically, when we consider the period of 1961–2010 as the whole training period and the period of 2011–2020 as the testing period, the EnNFSV-DA derives 15 perturbed forecasts from the lead-lag relationships established over five decades and 10 groups of multiple decades. By investigation, it is found that the ensemble mean of these perturbed forecasts promotes the lead time of skillful forecasts for the Niño3.4 index to more than 12 months from 5 months in the control forecast; furthermore, this ensemble mean generated by the EnNFSV-DA is shown to have the ability to recognize which type of El Niño will occur at least 8 months in advance. Additionally, the SPB phenomenon that severely limits the ENSO forecasting skill is obviously weaken by the EnNFSV-DA with an obviously slow decline in the ACC between the forecasts and observations and a significantly reduced error growth rates during the boreal spring. The EnNFSV-DA also performs much better than the NFSV-DA; in particular, the former further reduces the effect of the SPB and prolongs the skillful lead time for the Niño3.4 index to more than 12 months from 9 months in the latter'; furthermore, the former provides tropical SSTA patterns that are more similar to the observed ones for the two types of El Niño events. All these results indicate that useful precursory signals can be extracted from different decades by the EnNFSV-DA and then regarded as the indicators of

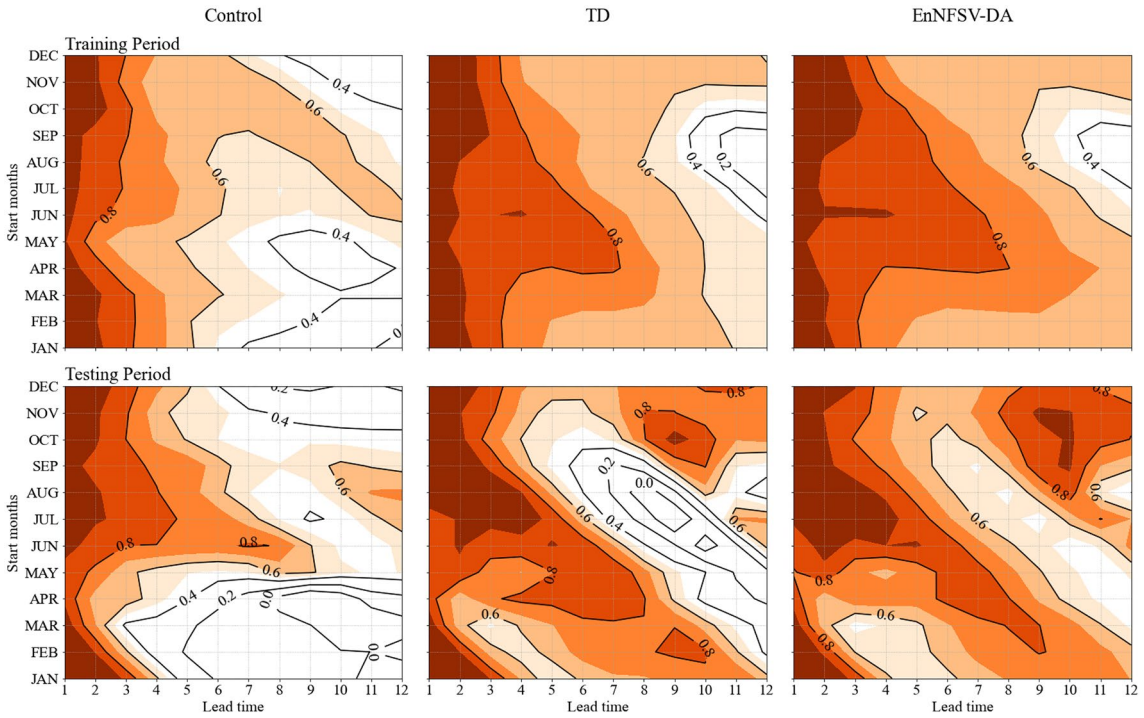

Fig. 11 ACC of predicted Niño3.4 index as a function of start and lead times for the control forecast, TD, and EnNFSV-DA during the training period of 1961–2010 and the testing period of 2011–2020

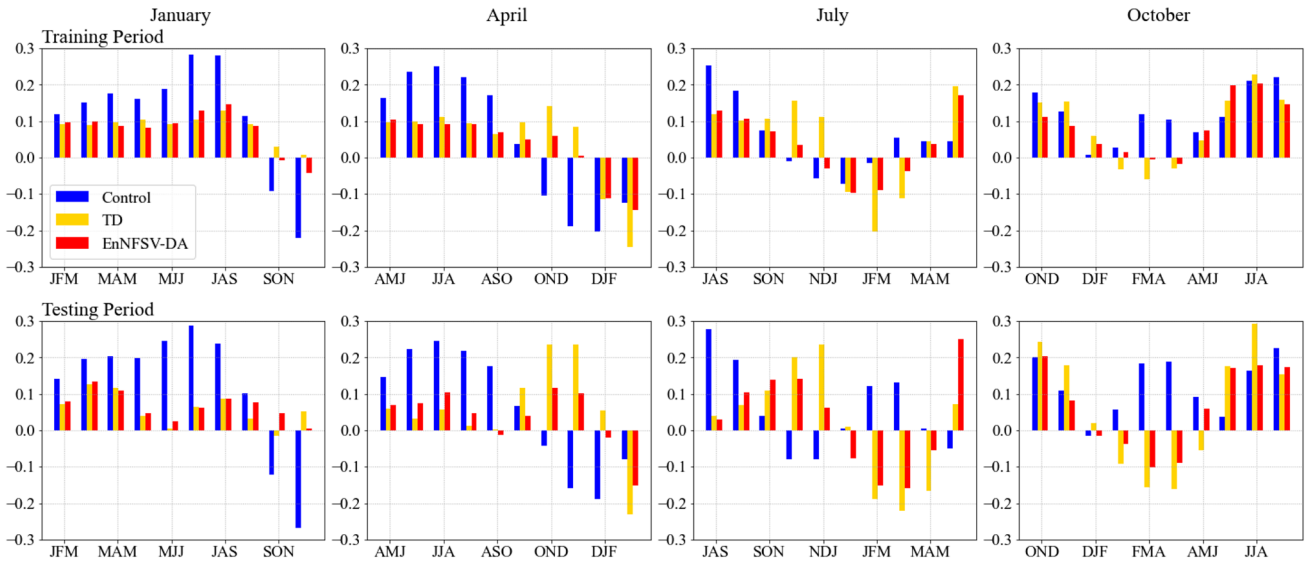

Fig. 12 Seasonal growth rate of prediction errors for the start months January, April, July, and October in the control forecast (blue bar), the TD (yellow bar) and the EnNFSV-DA (red bar) during the training period of 1961–2010 and the testing period of 2011–2020. The horizontal axis denotes the seasons and the vertical axis is the error growth rate

future SSTA predictions, finally promoting it to have a much higher forecasting skill. As far as what are these precursory signals, it would be further investigated. In fact, Yu and Kim (2011) and Hou et al. (2019) showed that the North Pacific variability dominates the development of the CP-El Niño and provides the precursory signal of the CP-El Nino. However, the Zebiak–Cane model only reproduces the tropical Pacific and does not include the extratropical forcing effect; now the ensemble of the NFSV-type tendency perturbations provided by the EnNFSV-DA may estimate much correctly

the Zebiak–Cane model bias originating from the absence of the extratropical forcing effect, then improving the skill of ENSO prediction. In any case, the EnNFSV-DA has the potential to become a promising approach for improving ENSO forecasting skill.

Presently, the EnNFSV-DA has been applied to ENSO forecasting. Although the Zebiak–Cane model adopted here is an intermediate model for ENSO, its results have encouraged us to apply the EnNFSV-DA to more realistic climate models for ENSO forecasting studies. It is expected that the EnNFSV-DA can extend its applications to other high-impact climate event forecasting. In addition, the SVD approach is used to extract the connection between the initial analysis SSTA and the NFSV-tendency perturbation. However, the SVD only addresses the linear mapping relationship and may omit the effect of nonlinearity on the connection. It is known that deep learning can resolve the nonlinear connection between two states; furthermore, its application is now ever-growing for numerical weather forecasting and climate prediction. Then, whether the deep learning approach can be used to diagnose the relationship between the analysis SSTA and NFSV-tendency perturbations and how well it works in improving ENSO forecasting skill should be explored in the future. Finally, it is noticed that the EnNFSV-DA is involved with neutralizing the prediction errors caused by both initial and model errors, which is distinct from the data assimilation (such as the four-dimension variational data assimilation) for only dealing with the initial error effect and is therefore much time-consuming. Then a much efficient algorithm for solving the EnNFSV-DA should be studied and its broad applications to numerical weather and climate predictions are expected.

Appendix

(1) Anomaly correlation coefficient (ACC)

The anomaly correlation coefficient (ACC) is used to test the deterministic prediction skills and is the correlation coefficient between the forecast anomaly and the observed anomaly. ACC is defined as Eq. (9).

$$ACC = \frac{\sum_{i=1}^{M}\left(O_i - \bar{O}_i\right)\left(x_i - \bar{x}_i\right)}{\sqrt{\sum_{i=1}^{M}\left(O_i - \bar{O}_i\right)^2\left(x_i - \bar{x}_i\right)^2}}, \tag{9}$$

where O_i is the observed anomaly, x_i is the forecast anomaly, and $\bar{O}_i$ and $\bar{x}_i$ are the time averages of the observation and forecast, respectively. M is the total length of time. The larger the ACC is, the higher the forecasting skill. It is generally considered that when ACC > 0.6, the forecast is skillful.

(B) Root mean square error (RMSE)

The root mean square error is also used to test deterministic forecasting skills, and it gives the average magnitude of the error in forecasts that deviate from observations. The RMSE is defined as Eq. (10):

$$RMSE = \sqrt{\frac{1}{M}\sum_{i=1}^{M}\left(x_i - O_i\right)^2}, \tag{10}$$

where M is the number of forecast results, that is, the total time length, x_i is the result of the i^{th} forecast time, and O_i is the observation value of the i^{th} forecast time. The smaller the RMSE is, the smaller the forecast error, and the more accurate the forecast.

(C) Noise-to signal-ratio (NS)

The noise-to signal- (NS) ratio in the present study measures ratio of the RMSE of the forecasted SSTA to the observed SSTA, it is defined as Eq. (11)

$$\mathrm{NS} = \frac{\mathrm{RMSE}}{\sqrt{\frac{1}{M}\sum_{t=1}^{M} O_i^2}}, \tag{11}$$

where the RMSE, M, and O_i are all as in Root mean square error (RMSE).

(D) Seasonal growth rate

The seasonal growth rate of prediction errors is expressed as the slope k of the time-dependent prediction error $E(t)$, which is defined as Eq. (12)

$$k = \frac{\partial E(t)}{\partial t} = \lim_{\Delta t \to 0}\frac{E\left(t_0 + \Delta t\right) - E\left(t_0\right)}{\Delta t}, \tag{12}$$

where t is the lead time. For the predicted SSTA in the present study, the approximation $k \approx \frac{E\left(t_0+\Delta t\right)-E\left(t_0\right)}{\Delta t}$ is adopted, where Δt is 1 month.

Author contributions WD and YZ contributed to the conception of the study; YZ performed the experiment and the data analyses; YZ and WD prepared all figures and tables and wrote the manuscript; LT and JM helped perform the analysis with constructive discussions.

Funding The study was jointly supported by the National Natural Science Foundation of China (Grant Nos. 41930971 and 42288101).

Data availability The datasets generated and/or analyzed during the study are stored on computers at the State Key Laboratory of Numerical

Modeling for Atmospheric Sciences and Geophysical Fluid Dynamics (LASG; https://www.lasg.ac.cn) and will be available to researchers upon request.

Declarations

Conflict of interest The authors declare no competing interests.

References

Alexander MA, Blade I, Newman M, Lanzante JR, Lau NC, Scott JD (2002) The atmospheric bridge: the influence of ENSO teleconnections on air–sea interaction over the global oceans. J Clim 15:2205–2231. https://doi.org/10.1175/1520-0442(2002)015<2205:Tabtio>2.0.Co;2

Ashok K, Behera SK, Rao SA, Weng HY, Yamagata T (2007) El Nino Modoki and its possible teleconnection. J Geophys Res Oceans 112:27. https://doi.org/10.1029/2006jc003798

Barkmeijer J, Iversen T, Palmer TN (2003) Forcing singular vectors and other sensitive model structures. Q J R Meteorol Soc 129:2401–2423. https://doi.org/10.1256/qj.02.126

Barnston AG, Tippett MK, L'Heureux ML, Li SH, DeWitt DG (2012) Skill of real-time seasonal ENSO model predictions during 2002–11 is our capability increasing? Bull Amer Meteorol Soc 93:631–651. https://doi.org/10.1175/bams-d-11-00111.1

Birgin EG, Martinez JM, Raydan M (2000) Nonmonotone spectral projected gradient methods on convex sets Siam. J Optim 10:1196–1211. https://doi.org/10.1137/s1052623497330963

Blumenthal MB (1991) Predictability of a coupled ocean atmosphere model. J Clim 4:766–784. https://doi.org/10.1175/1520-0442(1991)004<0766:Poacom>2.0.Co;2

Bretherton CS, Smith C, Wallace JM (1992) An intercomparison of methods for finding coupled patterns in climate data. J Clim 5:541–560. https://doi.org/10.1175/1520-0442(1992)005<0541:Aiomff>2.0.Co;2

Cane MA (1984) Oceanographic events during El Niño. Science 222:1189–1195

Chen D, Cane MA (2008) El Nino prediction and predictability. J Comput Phys 227:3625–3640. https://doi.org/10.1016/j.jcp.2007.05.014

Chen DK, Zebiak SE, Cane MA, Busalacchi AJ (1997) Initialization and predictability of a coupled ENSO forecast model. Mon Weather Rev 125:773–788. https://doi.org/10.1175/1520-0493(1997)125<0773:Iapoac>2.0.Co;2

Chen D, Cane MA, Kaplan A, Zebiak SE, Huang DJ (2004) Predictability of El Nino over the past 148 years. Nature 428:733–736. https://doi.org/10.1038/nature02439

Duan WS, Wei C (2013) The 'spring predictability barrier' for ENSO predictions and its possible mechanism: results from a fully coupled model. Int J Climatol 33:1280–1292. https://doi.org/10.1002/joc.3513

Duan WS, Zhou FF (2013) Non-linear forcing singular vector of a two-dimensional quasi-geostrophic model. Tellus Ser A Dyn Meteorol Oceanol 65:20. https://doi.org/10.3402/tellusa.v65i0.18452

Duan WS, Zhao P (2015) Revealing the most disturbing tendency error of Zebiak–Cane model associated with El Nino predictions by nonlinear forcing singular vector approach. Clim Dyn 44:2351–2367. https://doi.org/10.1007/s00382-014-2369-0

Duan W, Mu M (2018) Predictability of El Niño–Southern oscillation events. Oxf Res Encycl Clim Sci. https://doi.org/10.1093/acrefore/9780190228620.013.80

Duan WS, Tian B, Xu H (2014) Simulations of two types of El Nino events by an optimal forcing vector approach. Clim Dyn 43:1677–1692. https://doi.org/10.1007/s00382-013-1993-4

Duan WS, Li XQ, Tian B (2018) Towards optimal observational array for dealing with challenges of El Nino-Southern oscillation predictions due to diversities of El Nino. Clim Dyn 51:3351–3368. https://doi.org/10.1007/s00382-018-4082-x

Duan WS, Feng R, Yang LC, Jiang L (2022) A new approach to data assimilation for numerical weather forecasting and climate prediction. J Appl Anal Comput 12:1007–1021. https://doi.org/10.11948/20220098

Gao C, Wu XR, Zhang RH (2016) Testing a four-dimensional variational data assimilation method using an improved intermediate coupled model for ENSO analysis and prediction. Adv Atmos Sci 33:875–888. https://doi.org/10.1007/s00376-016-5249-1

Ham YG, Kug JS (2012) How well do current climate models simulate two types of El Nino? Clim Dyn 39:383–398. https://doi.org/10.1007/s00382-011-1157-3

Hendon HH, Lim E, Wang GM, Alves O, Hudson D (2009) Prospects for predicting two flavors of El Nino. Geophys Res Lett 36:6. https://doi.org/10.1029/2009gl040100

Hou MY, Duan WS, Zhi XF (2019) Season-dependent predictability barrier for two types of El Nino revealed by an approach to data analysis for predictability. Clim Dyn 53:5561–5581. https://doi.org/10.1007/s00382-019-04888-w

Huang B et al (2017) NOAA extended reconstructed sea surface temperature (ERSST), version 5. NOAA Natl Cent Environ Inf 30:8179–8205

Jeong HI et al (2012) Assessment of the APCC coupled MME suite in predicting the distinctive climate impacts of two flavors of ENSO during boreal winter. Clim Dyn 39:475–493. https://doi.org/10.1007/s00382-012-1359-3

Kao HY, Yu JY (2009) Contrasting Eastern-Pacific and Central-Pacific types of. ENSO J Clim 22:615–632. https://doi.org/10.1175/2008jcli2309.1

Keenlyside N, Latif M, Botzet M, Jungclaus J, Schulzweida U (2005) A coupled method for initializing El Nino Southern Oscillation forecasts using sea surface temperature. Tellus Ser A Dyn Meteorol Oceanol 57:340–356. https://doi.org/10.1111/j.1600-0870.2005.00107.x

Kim ST, Yu JY, Kumar A, Wang H (2012) Examination of the two types of ENSO in the NCEP CFS model and its extratropical associations. Mon Weather Rev 140:1908–1923. https://doi.org/10.1175/mwr-d-11-00300.1

Kirtman BP, Zebiak SE (1997) ENSO simulation and prediction with a hybrid coupled model. Mon Weather Rev 125:2620–2641. https://doi.org/10.1175/1520-0493(1997)125<2620:Esapwa>2.0.Co;2

Kleeman R, Moore AM (1997) A theory for the limitation of ENSO predictability due to stochastic atmospheric transients. J Atmos Sci 54:753–767. https://doi.org/10.1175/1520-0469(1997)054<0753:Atftlo>2.0.Co;2

Kramer W, Dijkstra HA (2013) Optimal localized observations for advancing beyond the ENSO predictability barrier. Nonlinear Process Geophys 20:221–230. https://doi.org/10.5194/npg-20-221-2013

Kug JS, Jin FF, An SI (2009) Two types of El Nino events: Cold Tongue El Nino and warm Pool El. Nino J Clim 22:1499–1515. https://doi.org/10.1175/2008jcli2624.1

Langland RH (2005) Issues in targeted observing. Q J R Meteorol Soc 131:3409–3425. https://doi.org/10.1256/qj.05.130

Lopez H, Kirtman BP (2014) WWBs, ENSO predictability, the spring barrier and extreme events. J Geophys Res Atmos 119:25. https://doi.org/10.1002/2014jd021908

McPhaden MJ, Zebiak SE, Glantz MH (2006) ENSO as an integrating concept Earth Sci. Science 314:1740–1745. https://doi.org/10.1126/science.1132588

Moore AM, Kleeman R (1999) Stochastic forcing of ENSO by the intraseasonal oscillation. J Clim 12:1199–1220. https://doi.org/10.1175/1520-0442(1999)012<1199:Sfoebt>2.0.Co;2

Mu M, Duan WS, Chen DK, Yu WD (2015) Target observations for improving initialization of high-impact ocean-atmospheric environmental events forecasting. Natl Sci Rev 2:226–236. https://doi.org/10.1093/nsr/nwv021

Murphy AH, Epstein ES (1989) Skill scores and correlation-coefficients in model verification. Mon Weather Rev 117:572–581. https://doi.org/10.1175/1520-0493(1989)117<0572:SSACCI>2.0.CO;2

Nicolis C, Perdigao RAP, Vannitsem S (2009) Dynamics of prediction errors under the combined effect of initial Condition and Model errors. J Atmos Sci 66:766–778. https://doi.org/10.1175/2008jas2781.1

Qi QQ, Duan WS, Zheng F, Tang YM (2017) On the "spring predictability barrier" for strong El Nio events as derived from an intermediate coupled model ensemble prediction system. Sci China Earth Sci 60:1614–1631. https://doi.org/10.1007/s11430-017-9087-2

Ren HL, Zuo JQ, Deng Y (2019) Statistical predictability of Nino indices for two types of. ENSO Clim Dyn 52:5361–5382. https://doi.org/10.1007/s00382-018-4453-3

Snyder C (1996) Summary of an informal workshop on adaptive observations and FASTEX. Bull Amer Meteorol Soc 77:953–961

Tang YM, Kleeman R, Moore AM (2004) SST assimilation experiments in a tropical Pacific Ocean model. J Phys Oceanogr 34:623–642. https://doi.org/10.1175/3518.1

Tang YM, Deng ZW, Zhou XB, Cheng YJ, Chen D (2008) Interdecadal variation of ENSO predictability in multiple models. J Clim 21:4811–4833. https://doi.org/10.1175/2008jcli2193.1

Tang YM et al (2018) Progress in ENSO prediction and predictability study. Natl Sci Rev 5:826–839. https://doi.org/10.1093/nsr/nwy105

Tao LJ, Duan WS (2019) Using a nonlinear forcing singular vector approach to reduce model error effects in ENSO. Forecast Weather Forecast 34:1321–1342. https://doi.org/10.1175/waf-d-19-0050.1

Tao LJ, Gao C, Zhang RH (2019) Model parameter-related optimal perturbations and their contributions to El Nino prediction errors. Clim Dyn 52:1425–1441. https://doi.org/10.1007/s00382-018-4202-7

Tao LJ, Duan WS, Vannitsem S (2020) Improving forecasts of El Nino diversity: a nonlinear forcing singular vector approach. Clim Dyn 55:739–754. https://doi.org/10.1007/s00382-020-05292-5

Tao LJ, Duan WS, Jiang L (2022) Model errors of an intermediate model and their effects on realistic predictions of El Nino diversity. Int J Climatol. https://doi.org/10.1002/joc.7656

Vannitsem S, Toth Z (2002) Short-term dynamics of model errors. J Atmos Sci 59:2594–2604. https://doi.org/10.1175/1520-0469(2002)059<2594:Stdome>2.0.Co;2

Webster PJ, Yang S (1992) Monsoon and ENSO—selectively interactive systems. Q J R Meteorol Soc 118:877–926. https://doi.org/10.1256/smsqj.50704

Wu DH, Anderson DLT, Davey MK (1993) ENSO variability and external impacts. J Clim 6:1703–1717. https://doi.org/10.1175/1520-0442(1993)006<1703:Evaei>2.0.Co;2

Xu H, Duan WS, Wang JC, IEEE (2006) The tangent linear model and adjoint of a coupled ocean-atmosphere model and its application to the predictability of ENSO. In: IEEE International Geoscience and Remote Sensing Symposium (IGARSS), Denver, CO, Jul 31–Aug 04 2006. IEEE International Symposium on Geoscience and Remote Sensing IGARSS. pp 640-+.https://doi.org/10.1109/igarss.2006.168

Xue Y, Cane MA, Zebiak SE, Blumenthal MB (1994) On the prediction of ENSO—a study with a low-order Markov model. Tellus Ser A Dyn Meteorol Oceanol 46:512–528. https://doi.org/10.1034/j.1600-0870.1994.00013.x

Yu JY, Kim ST (2011) Relationships between extratropical sea level pressure variations and the central Pacific and Eastern Pacific types of ENSO. J Clim 24:708–720. https://doi.org/10.1175/2010jcli3688.1

Yu LS, Weller RA, Liu WT (2003) Case analysis of a role of ENSO in regulating the generation of westerly wind bursts in the Western Equatorial Pacific. J Geophys Res Oceans 108:20. https://doi.org/10.1029/2002jc001498

Zebiak SE, Cane MA (1987) A model el niñ–southern oscillation. Mon Weather Rev 115:2262–2278

Zheng F, Yu JY (2017) Contrasting the skills and biases of deterministic predictions for the two types of El Nino. Adv Atmos Sci 34:1395–1403. https://doi.org/10.1007/s00376-017-6324-y